Pattern Recognition (2016) ....
[Down Sci Direct on http://www.sciencedirect.com/science/article/pii/S003132031600042X]
"Active contours textural and inhomogeneous object extraction",
by L Mabood, Haider Ali, Noor Badshah, Ke Chen, G Khan, Vol 55, 87-99

Active Contours Textural and Inhomogeneous Object Extraction

Lutful Mabood[*], *Haider Ali*[†], *Noor Badshah*[‡], *Ke-Chen*[§], *Gulzar Ali Khan*[¶]

Abstract

A new selective segmentation active contour model is proposed in this paper that embeds an enhanced image information. By utilizing the average image of channels (AIC), which handles texture and noise, our model is capable to selectively segment and capture objects with nonuniform features. Moreover, the AIC is fitted with linear functions which are updated regularly to accurately guide the level set function to handle non constant intensities. Furthermore, we employ prior information in terms of geometrical constraints which work in alliance with image information to capture objects with intensity inhomogeneity. Experiments show that the proposed method achieves better results than the latest selective segmentation models. In addition, our approach maintains the performance on some hard real and synthetic color images.

Keywords. Image selective segmentation, Level set, Functional minimization, Numerical method.

1 Introduction

Image segmentation is one of the most important and complicated task in the field of image processing and computer vision. Many different approaches are introduced in the literature including PDE-based active contour models [8, 14] for curve evolution which has gained much popularity among the researchers. The active contour methods use a partial differential equation (PDE) to model and track how fronts evolve in a discrete domain by maintaining and updating a distance field to the fronts. This method can be categorized as the edge-based methods [3, 4, 11, 12] and region-based methods [9, 18, 22, 28]. The edge-based models use edge information to guide the active contours towards the object boundaries, whereas, region based models use statistical region data of an image. In particular, the Mumford-Shah (MS) model [18] is a milestone in the region based segmentation models.

[*]Department of Mathematics, University of Peshawar. email. lathizm@gmail.com
[†]Department of Mathematics, University of Peshawar. email. haider_uop99@yahoo.com
[‡]Department of Basic Sciences, UET Peshawar. email. noor2knoor@gmail.com
[§]Department of Mathematical Sciences, The University of Liverpool, UK. email. k.chen@liv.ac.uk
[¶]Department of Mathematics, University of Peshawar. email. mshahkar95@yahoo.com

For a given image $z = z(x, y)$, the MS model for segmentation solves

$$\min_{z_0,\Gamma} F(z_0, \Gamma)^{MS} = \mathcal{H}^{n-1}(\Gamma) + \parallel z - z_0 \parallel^2_{L_2(\Omega)} + \alpha \int_{\Omega-\Gamma} |\nabla z_0|^2 dxdy \tag{1}$$

for the reconstruction of the ideal image $z_0(x, y)$ over domain Ω, where Ω is a bounded subset of $\mathbb{R}^n$ with Lipschitz boundary and the feature boundary set Γ. The term $\mathcal{H}^{n-1}$ is the $n-1$ dimensional Hausdorff measure, which in the 2-dimensional case $\mathcal{H}^1$ denotes the length of the curve. Since the term $\mathcal{H}^{n-1}$ causes computational complexity in the MS functional, therefore a natural way to approximate MS functional was introduced by Chan-Vese (CV) [9], which implemented the piecewise segmentation

$$F^{2D}_{CV}(\Gamma, c_1, c_2) = \mu.\mathcal{H}^1(\Gamma) + \lambda_1 \parallel z - c_1 \parallel^2_{L_2(\Omega_{in})} + \lambda_2 \parallel z - c_2 \parallel^2_{L_2(\Omega_{out})}, \tag{2}$$

where c_1 and c_2 are average values of z respectively in Ω_{in} (i.e., inside Γ) and in (Ω_{out}) (i.e., outside of Γ). In level set formulation the equation (2) takes the form

$$F^{2D}_{CV}(\phi, c_1, c_2) = \mu\mathcal{H}^1(\phi) + \lambda_1 \parallel z - c_1 \parallel^2_{L_2(\Omega_{in})} + \lambda_2 \parallel z - c_2 \parallel^2_{L_2(\Omega_{out})},$$

where

$$\begin{aligned} \mathcal{H}^1(\phi) &= \int_\Omega \delta(\phi)|\nabla\phi| dxdy, && (3)\\ \parallel z - c_1 \parallel^2_{L_2(\Omega_{in})} &= \int_\Omega |z(x, y) - c_1|^2 H(\phi) dxdy, && (4)\\ \parallel z - c_2 \parallel^2_{L_2(\Omega_{out})} &= \int_\Omega |z(x, y) - c_2|^2 (1 - H(\phi)) dxdy. && (5) \end{aligned}$$

Since the Heaviside function, H, is not differentiable at the origin, a regularized version of Heaviside function is used [9, 10, 20],

$$H_\epsilon(w) = \frac{1}{2}\Big(1 + \frac{2}{\pi}\arctan(\frac{w}{\epsilon})\Big), \qquad \delta_\epsilon(w) = H'_\epsilon(w) = \frac{\epsilon}{\pi(\epsilon^2 + w^2)}. \tag{6}$$

A simple extension to the CV model is to use linear approximation instead of constant [23]. This model is more appropriate when the image has region of linear shading instead of piecewise constant intensities.

$$\begin{aligned} F^{2D}_{Linear}(\phi, a_i, b_i) &= \mu.\mathcal{H}^1(\phi) + \lambda_1 \parallel z - (a_0 + a_1 x + a_2 y) \parallel^2_{L_2(\Omega_{in})} \\ &+ \lambda_2 \parallel z - (b_0 + b_1 x + b_2 y) \parallel^2_{L_2(\Omega_{out})} \end{aligned} \tag{7}$$

where a_i, b_i, where $i = 0, 1, 2$ are coefficients of linear functions. The a_i can be computed by linear system:

$$\frac{\partial}{\partial a_i} \parallel z - (a_0 + a_1 x + a_2 y) \parallel^2_{L_2(\Omega_{in})} = 0, i = 0, 1, 2, \tag{8}$$

whereas similar solution procedure follows for b_i. Several recent generalization and variants [2, 16, 15, 19, 25, 26] of the CV model can be seen which have shown better results in bias field correction, texture and noise. However, these aforementioned segmentation models are not designed for segmenting a particular object of interest and not all objects in it. Thus selective segmentation is a task in which an object/region of interest is detected, given additional information of geometric constraints in the form of list of points near the object/region. Motivated from the work in [11, 12], we recently proposed two mixed models of edge based and region-based methods that are more robust for noisy images [3] and when edges are not prominent[4]. However, these models were not designed for texture and inhomogeneity.

In this paper, we propose a novel active contour model (ACM) which embeds AIC, an enhanced version of a given image for robust guidance of the contour to capture, objects with diffuse edges, objects with noise and textural detail. Furthermore, the AIC is approximated with linear functions to handle varying intensity objects. Experiments show that the proposed method achieves better results than the latest selective segmentation models. Moreover, the proposed approach maintains the performance in real and synthetic color images.

The rest of the paper is organized as follows. Section 2 reviews some latest selective segmentation models. Section 3 exhibits the proposed new model. Section 4 reveals an additive operator splitting (AOS) method for solving the resulted PDE. Section 5 displays some experimental tests with competing models. Conclusion is made in Section 6.

2 The Badshah-Chen Model (BC)

To capture a particular object of interest, the Badshah and Chen (BC) [3] proposed the following functional for minimization

$$F^{2D}_{BC}(\phi, c_1, c_2) \;=\; \mu\mathcal{H}^1_{dg}(\phi) + \lambda_1 \parallel z - c_1 \parallel^2_{L_2(\Omega_{in})} + \lambda_2 \parallel z - c_2 \parallel^2_{L_2(\Omega_{out})} .$$

The term $\mathcal{H}^1_{dg}(\phi)$ is weighted length term, weighted with an edge detector function g [3, 4] and a distance function d given by

$$d(x,y) = \prod_{i=1}^{n} \left(1 - e^{-\frac{(x-x_i)^2}{2\sigma^2}} e^{-\frac{(y-y_i)^2}{2\sigma^2}}\right), \qquad \forall (x,y) \in \Omega, \tag{9}$$

where $\{(x_i, y_i) : i = 1, 2, 3, ..., m\}$ are the points around the object of interest.

The BC model [3] is the state of the art model which overcomes the deficiencies of the Gout model [11]. On one side the BC model is working well in noisy images and on the other side it is robust in terms of CPU time and number of iterations [3, 4]. However there are images which are challenging for the BC model, such as MRI and CT images with fuzzy edges, unilluminated organs and overlapping homogeneous regions [4]. To overcome this problem a new model was introduced which is based on the concept of coefficient of variation (CoV) [4].

3 Coefficient of Variation Equipped Selective Segmentation Model (SSM)

The coefficient of variation (CoV) based image selective segmentation model [4] in level set formulation [27] is given by:

$$F^{2D}_{COV}(\phi, c_1, c_2) \;=\; \mu\mathcal{H}^1_{dg}(\phi) + \lambda_1 \parallel \frac{z-c_1}{c_1} \parallel^2_{L_2(\Omega_{in})} + \lambda_2 \parallel \frac{z-c_2}{c_2} \parallel^2_{L_2(\Omega_{out})} . \tag{10}$$

Minimization of $F^{2D}_{COV}(\phi, c_1, c_2)$ leads to the following equations for the solutions c_1, c_2 and ϕ respectively as

$$c_1(\phi) = \frac{\parallel z \parallel^2_{L_2(\Omega_{in})}}{\parallel \sqrt{z} \parallel^2_{L_2(\Omega_{in})}} \qquad c_2(\phi) = \frac{\parallel z \parallel^2_{L_2(\Omega_{out})}}{\parallel \sqrt{z} \parallel^2_{L_2(\Omega_{out})}}, \tag{11}$$

and

$$\begin{cases} \delta_\epsilon(\phi)\Big[\mu \mathrm{div}\Big(G(x,y)\frac{\nabla\phi}{|\nabla\phi|}\Big) \\ -\lambda_1\dfrac{(z(x,y)-c_1)^2}{c_1^2} + \lambda_2\dfrac{(z(x,y)-c_2)^2}{c_2^2}\Big] = 0 & \text{in } \Omega, \\ \dfrac{G(x,y)\delta_\epsilon(\phi)}{|\nabla\phi|}\dfrac{\partial\phi}{\partial\vec{n}} = 0 & \text{on } \partial\Omega, \end{cases} \tag{12}$$

where

$$G(x,y) = d(x,y)g(|\nabla z|). \tag{13}$$

After adding a balloon term $\alpha G(x,y)|\nabla\phi|$ as done in [3] to speed up the convergence, the evolution equation is obtained as follows:

$$\begin{aligned} \frac{\partial\phi}{\partial t} &= \delta_\epsilon(\phi)\Big[\mu\nabla.\Big(G(x,y)\frac{\nabla\phi}{|\nabla\phi|}\Big) - \lambda_1\frac{(z(x,y)-c_1)^2}{c_1^2} \\ &+ \lambda_2\frac{(z(x,y)-c_2)^2}{c_2^2} + \alpha G(x,y)|\nabla\phi|\Big], \quad in\ \Omega \end{aligned} \tag{14}$$

$$\phi(t,x,y) = \phi_0(x,y), \quad in\ \Omega. \tag{15}$$

Although the SSM model works well in images having objects of diffuse edges or low contrast type of objects [4], but still on the other hand segmenting textural objects is an issue for both BC and SSM model. To overcome this issue, we propose a new model based on the concept of AIC.

4 The Proposed Model (MABC Model)

The idea behind the AIC model is to utilize more convenient form of a given image data to accurately guide the level set function for efficient segmentation of images having texture and noise. To obtain the AIC, we will utilize the extended structure tensor (EST) which

is an extended version of the classical structure tensor for the texture image segmentation. We explain the basic idea behind our approach as follows.
For a given gray image $z(x, y)$ the classical structure tensor (CST) J_σ is obtained by Gaussian smoothing of the tensor product of the image gradient, i.e.,

$$J_\sigma = K_\sigma * (\nabla z \nabla z^T) = \begin{pmatrix} K_\sigma * z_x^2 & K_\sigma * z_x z_y \\ K_\sigma * z_x z_y & K_\sigma * z_y^2 \end{pmatrix} \tag{16}$$

where K_σ is a Gaussian kernel with standard deviation σ, and subscripts x and y denote the partial derivatives. For vector-valued images, the following expression is employed:

$$J_\sigma = K_\sigma * \Big(\sum_{i=1}^{n} \nabla z_i \nabla z_i^T \Big).$$

For a gray scale image $z(x, y)$ the extended structure tensor $(EST) J_\sigma^E$ is define as:

$$J_\sigma^E = K_\sigma * (uu^T) = \begin{pmatrix} K_\sigma * z_x^2 & K_\sigma * z_x z_y & K_\sigma * z_x z \\ K_\sigma * z_x z_y & K_\sigma * z_y^2 & K_\sigma * z_y z \\ K_\sigma * z_x z & K_\sigma * z_y z & K_\sigma * z^2 \end{pmatrix} \tag{17}$$

where

$$u = \begin{bmatrix} z_x & z_y & z \end{bmatrix}^T$$

For vector-valued images, the following expression can be used:

$$J_\sigma^E = K_\sigma * \Big(\sum_{i=1}^{N} u_i u_i^T \Big)$$

where

$$u_i = \begin{bmatrix} z_{i,x} & z_{i,y} & z_i \end{bmatrix}^T$$

As it is clear from equation (16) that the CST yields three feature channels for each scale i.e., z_x^2, z_y^2, and $z_x z_y$. While, it is clear from equation (17) that EST uses six feature channels instead of three in which three of them contain the original image information. This makes the use of EST more convenient as compared to CST, the reason behind this is that: the classical structure tensor has the disadvantage of not using any intensity information i.e. it uses only three feature channel and does not use the original image data which may give the resultant image far different than the given image. For instant, see the Fig. 1 where for the given images in Fig. 1(a), 1(d) and 1(g), the CST performance can be seen respectively as Fig. 1(b), 1(e) and 1(h). It can be very easily observed that by using CST, the results are not satisfactory. On the other hand, if the intensity information is incorporated into CST to get EST, the results which are much better can be seen in Fig. 1(c), 1(f) and 1(i).
Thus we will first compute the EST and then obtain the AIC, average image of all the channels $J_{\sigma,i}^E (i = 1, 2...9)$ belonging to the EST J_σ^E. The AIC denoted by $z^\star$ is given by

$$z^\star = \frac{1}{9} \sum_{i=1}^{9} J_{\sigma,i}^E \tag{18}$$

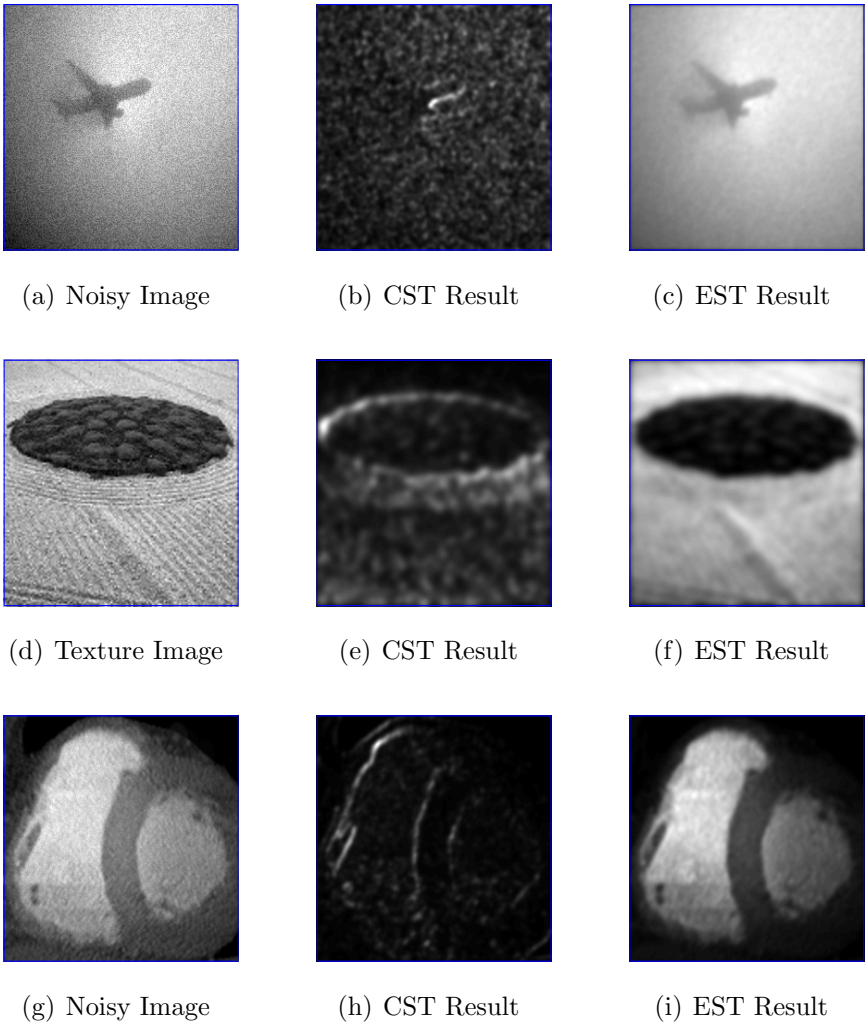

(a) Noisy Image (b) CST Result (c) EST Result

(d) Texture Image (e) CST Result (f) EST Result

(g) Noisy Image (h) CST Result (i) EST Result

Fig. 1: The figure illustrating results of CST and EST on noisy and textural images. (a) Given noisy Image; (b) CST result; (c) EST result; (d) Given textural image (e) CST result (f) EST result; (g) Given noisy image; (h) CST result; (i) EST result.

where σ is the standard deviation of Gaussian kernel. The image $z^{\star}(x, y)$ is a blend of classical structure tensor and original image information which helps to smooth textural features by maintaining image original features [28]. Since the use of Gaussian smoothing causes the edge diffusion in EST, therefore selection of an efficient fidelity term is a crucial step.

We propose the following functional of minimization for selective segmentation

$$F_{MABC}^{2D} = \mu \mathcal{H}_{dg}^{1}(\phi) + \lambda D(z^{\star}(x, y)). \tag{19}$$

The first term in the above functional is a blend of metric and edge detector function. The metric function serves as a prior information by restricting the contour around the object of interest for selective segmentation and tries to avoid influence of intensity inhomogeneity. The edge detector function attracts the contour towards the true boundaries of the object of interest using the image original information in the form of gradient. The second term is the data term which uses the information from the AIC to tackle textural and noisy object of interest. On the other hand, the AIC creates diffusion near the object edges during smoothing process and therefore, the incorporation of a suitable data fitting term is also required. For the data term $D_{term}(z^{\star}(x, y))$ in our proposed model (19), we consider two options, namely, piecewise constant [3, 9, 22] and piecewise linear [23] approximation of the AIC and are respectively as follows:

$$D_{constant} = \| z^{\star} - c_1 \|_{L_2(\Omega_{in})}^2 + \lambda_2 \| z^{\star} - c_2 \|_{L_2(\Omega_{out})}^2, \tag{20}$$

and

$$\begin{aligned} D_{linear} &= \lambda_1 \| z^{\star} - (a_0 + a_1 x + a_2 y) \|_{L_2(\Omega_{in})}^2 \\ &+ \lambda_2 \| z^{\star} - (b_0 + b_1 x + b_2 y) \|_{L_2(\Omega_{out})}^2 . \end{aligned} \tag{21}$$

It can be seen from figure 2 that the data term $D_{constant}$ is good in detecting constant intensity objects whereas the performance is poor in inhomogeneous intensity objects. On the other hand, the data term D_{linear} is performing good in detecting objects of variable intensities.

Therefore, the proposed functional in level set formulation (19) with linear fidelity term is as follows

$$F_{MABC}^{2D} = \mu \mathcal{H}_{dg}^{1}(\phi) + \lambda D_{linear}(z^{\star}(x, y)), \tag{22}$$

The minimization of the proposed functional (22) yields the following equations for solutions a_i, b_i and ϕ, respectively

$$\frac{\partial}{\partial a_i} \| z^{\star}(x, y) - (a_0 + a_1 x + a_2 y) \|_{L_2(\Omega_{in})}^2 = 0, i = 0, 1, 2, \tag{23}$$

$$\frac{\partial}{\partial b_i} \| z^{\star}(x, y) - (b_0 + b_1 x + b_2 y) \|_{L_2(\Omega_{in})}^2 = 0, i = 0, 1, 2, \tag{24}$$

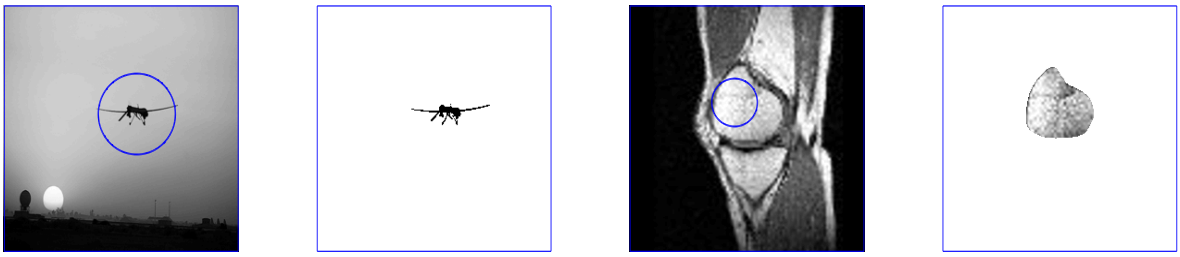

(a) Initial Contour (b) $D_{constant}$ Result (c) Initial Contour (d) $D_{constant}$ Result

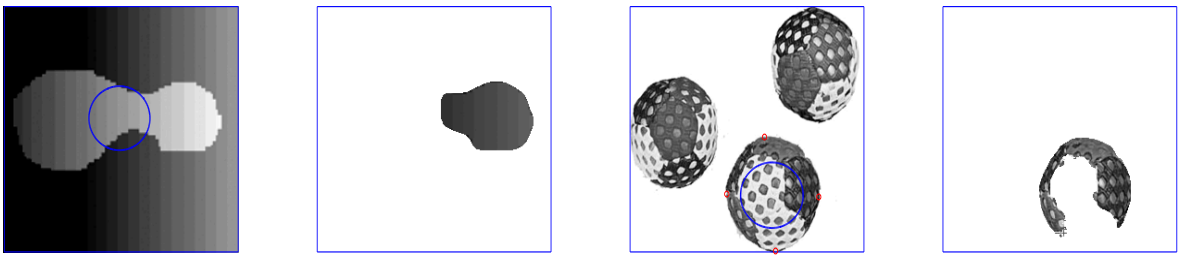

(e) Initial Contour (f) $D_{constant}$ Result (g) Initial Contour (h) $D_{constant}$ Result

Fig. 2: The figure illustrating the performance of the data term $D_{constant}$. (Row 1st) The successful detection by the data term $D_{constant}$; (Row 2nd) The unsuccessful detection by the data term $D_{constant}$.

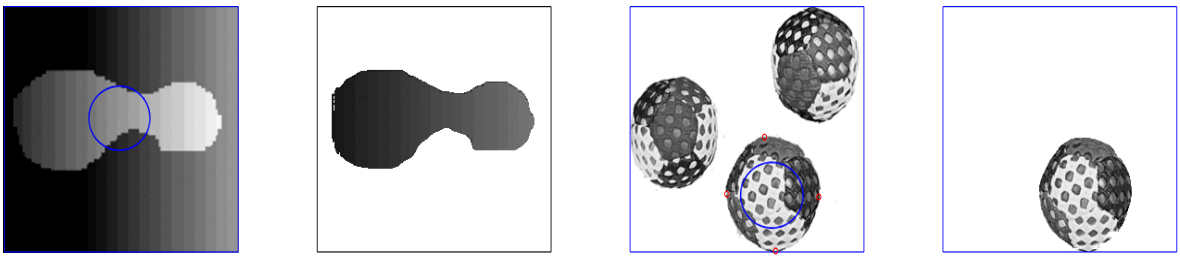

(a) Initial Contour (b) D_{linear} Result (c) Initial Contour (d) D_{linear} Result

Fig. 3: The figure illustrating the performance of the data term D_{linear}. (a) Object of interest; (b) Object extracted; (c) The object of interest; (d) The successful result by using D_{linear}.

and

$$\frac{\partial \phi}{\partial t} = \delta_\epsilon(\phi)\Big[\mu\nabla.\Big(G(x,y)\frac{\nabla\phi}{|\nabla\phi|}\Big) - D_{linear}(z^\star(x,y))\Big], \quad in\ \Omega \tag{25}$$

$$\phi(t,x,y) = \phi_0(x,y), \quad in\ \Omega. \tag{26}$$

We solve the above PDE by using Additive Operating Method as done in [3].

5 Experimental Results

This section exhibits some test results of the proposed model and latest selective segmentation models. First we compare the results of the proposed model with the Gout model on some synthetic and real world images. Secondly, we test the proposed model, BC and SSM models on some real and synthetic images. Finally, we test the proposed model on color noisy and textural real world and synthetic hard images. The proposed model is implemented using Matlab 7.9.0 on a core i3 computer with 2GB RAM, 2.40 GHz processer, and window 7 operating system. In all the three models we use $\lambda_1 = \lambda_2 = \lambda$.
We first test the proposed model and the Gout model on a noisy synthetic image as displayed in Fig. 4(a). It can be very easily observed that the Gout model is unable to capture the object of interest whereas the proposed model completed the desired task successfully in figure 4(f). Next, Fig. 5 shows a medical brain image in which a tumor is to be segmented but it is clear from figure 5(c) that Gout model is not able to segment it. In contrast the figure 5(g) shows the successful attempt by the proposed model. Similarly, Fig. 6 exhibits a noisy medical image of a knee in which a particular bone is to be segmented. From the figure 6(c), it can be easily seen that the Gout model is unable to complete the task. On the other hand, the proposed model completed the desired task efficiently which can be seen in Fig. 6(g). Now we compare the new model with the BC and the SSM model. For brevity, we shall denote:
M-1 — the BC model
M-2 — the SSM model and
M-3 — the proposed MABC.
We begin with some simple examples where all three (M-1,M-2 and M-3) work well and then give some examples of textural, noisy and other hard images that will show that M-3 has far better performance than the M-1 and M-2.
In each of the following figures, the performance of the M-1, M-2, and the proposed M-3 can be seen in row first, second, and third respectively. The first column shows the original image with initial contours. The second column displays the intermediate situations of active contour of each model. The third column reveals the final solution in each model and the fourth column displays the segmented version of the final solution for the sake of convenience in deep observations.
In figure 7(a) the original image with initial contour is displayed. The figure 7(c) and 7(g) shows that M-1 model and M-2 are unable to complete the task while the successful

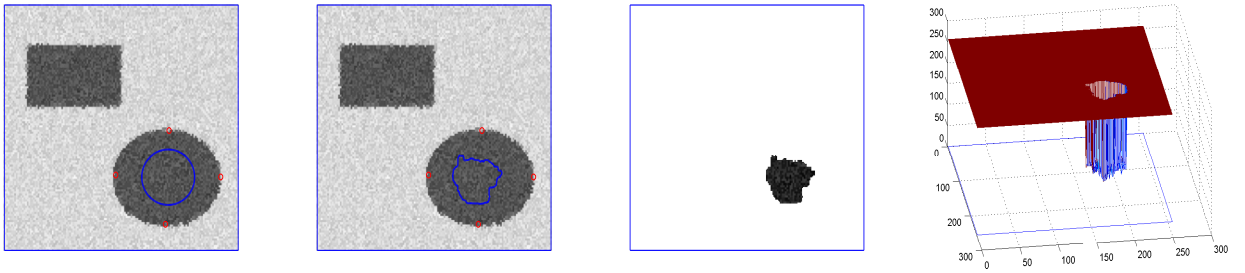

(a) Initial Contour (b) Gout Model (c) Segmented Result (d) Corresponding 3D Graph

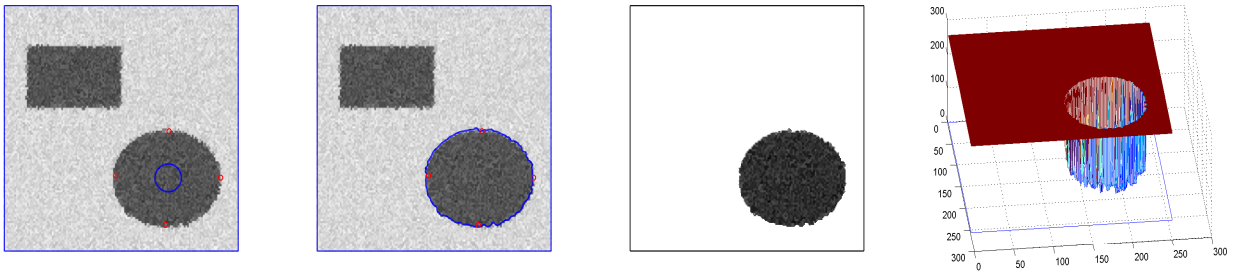

(e) Initial Contour (f) Proposed Model (g) Segmented Result (h) Corresponding 3D Graph

Fig. 4: A figure illustrating the performance of Gout model (first row) and proposed model (second row) on noisy image. In contrast with Gout model, the Proposed model successfully completed the task as clear from 4(g).

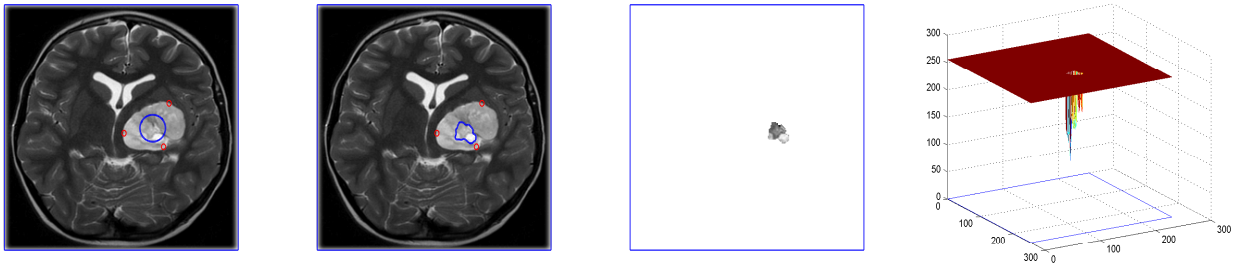

(a) Initial Contour (b) Gout Model (c) Segmented Result (d) Corresponding 3D Graph

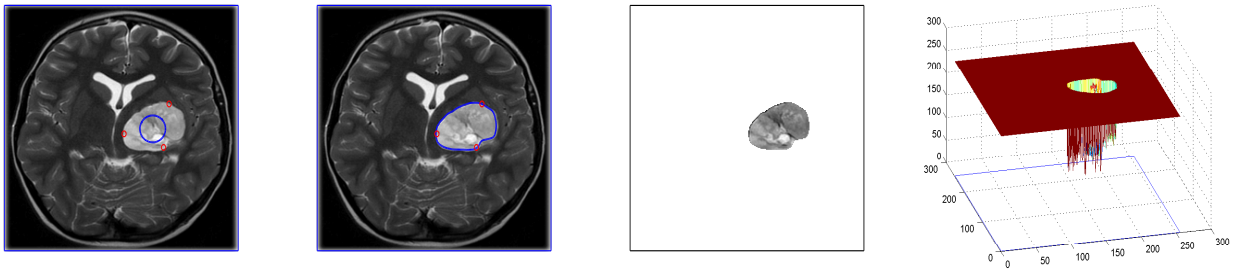

(e) Initial Contour (f) Proposed Model (g) Segmented Result (h) Corresponding 3D Graph

Fig. 5: A figure illustrating the performance of Gout model (first row) and proposed model (second row) on real medical brain image. In contrast to Gout model, the Proposed model successfully captured the region of interest.

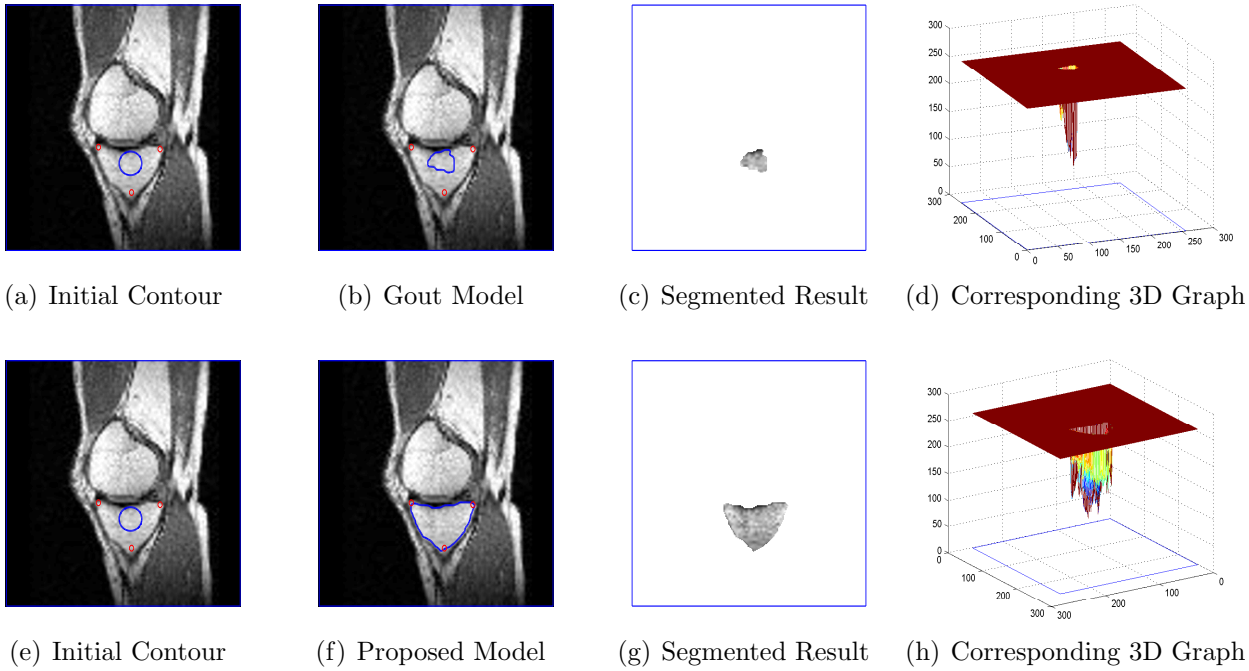

(a) Initial Contour (b) Gout Model (c) Segmented Result (d) Corresponding 3D Graph

(e) Initial Contour (f) Proposed Model (g) Segmented Result (h) Corresponding 3D Graph

Fig. 6: A figure illustrating the performance of Gout model (first row) and proposed model (second row) on real medical knee image. In contrast to Gout model, the Proposed model successfully captured the region of interest.

result of M-3 can be seen clear from 7(k). The figure 8 shows a real world image in which the uncompleted result of M-2 can be seen from 8(g). On the other hand, the successful detection by M-3 model can easily observed from the same figure. The figure 9 exhibits a real medical abdominal image with Poisson noise. The figure 9(c) shows the uncompleted task of M-1 model. Although, it can be seen in 9(g) and 9(l) that M-2 detected the desired region but it should also be noted that M-2 took 520 iterations while M-3 completed the job in 200 iterations.

The figure 10 exhibits a synthetic inhomogeneous image. It can be easily observed from the same figure that M-1 and M-2 are unable to capture the inhomogeneous intensity object while the proposed M-3 successfully captured the object. Next,the three models are tested on some textural intensity images. For example, the figures 11, 12, 13 and 14 are textural images in which M-1 and M-2 are completely unable to work due to the textural objects. The uncompleted tasks of M-1 and M-2 are shown in figures 11(c), 12(c), 13(c), 14(c) and 11(g), 12(g), 13(g), 14(g). While the successful results of M-3 in texture images can be seen in figures 11(k), 12(k), 13(k) and 14(k). Firstly, in figure 11, the three models are tested on a real snake image in desert. The robust performance of the proposed M-3 can be easily witnessed from the same figure, while, the uncomplete tasks of M-1 and M-2 are also displayed. Next, the three models are tested on a synthetic textural image as in figure 12. It can be easily observed from the figure that the proposed model captured completely the object of interest by handling successfully the texture information on the

object. On the other hand, the unsuccessful performance by M-1 and M-2 can also be seen from the same figure. Next, the three models are tested on a real world image as in figure 13 displaying three balls with interior textural details. The successful attempt by M-3 and unsuccessful attempts by M-1 and M-2 can easily witnessed from the same figure. The M-3 model successfully captured the selected ball by ignoring the textural details on the ball. Next, all the three models are tested on a real world image displaying six textural objects as in figure 14. It can be easily observed that the proposed M-3 successfully captured the textural object of interest in contrast to M-1 and M-2.

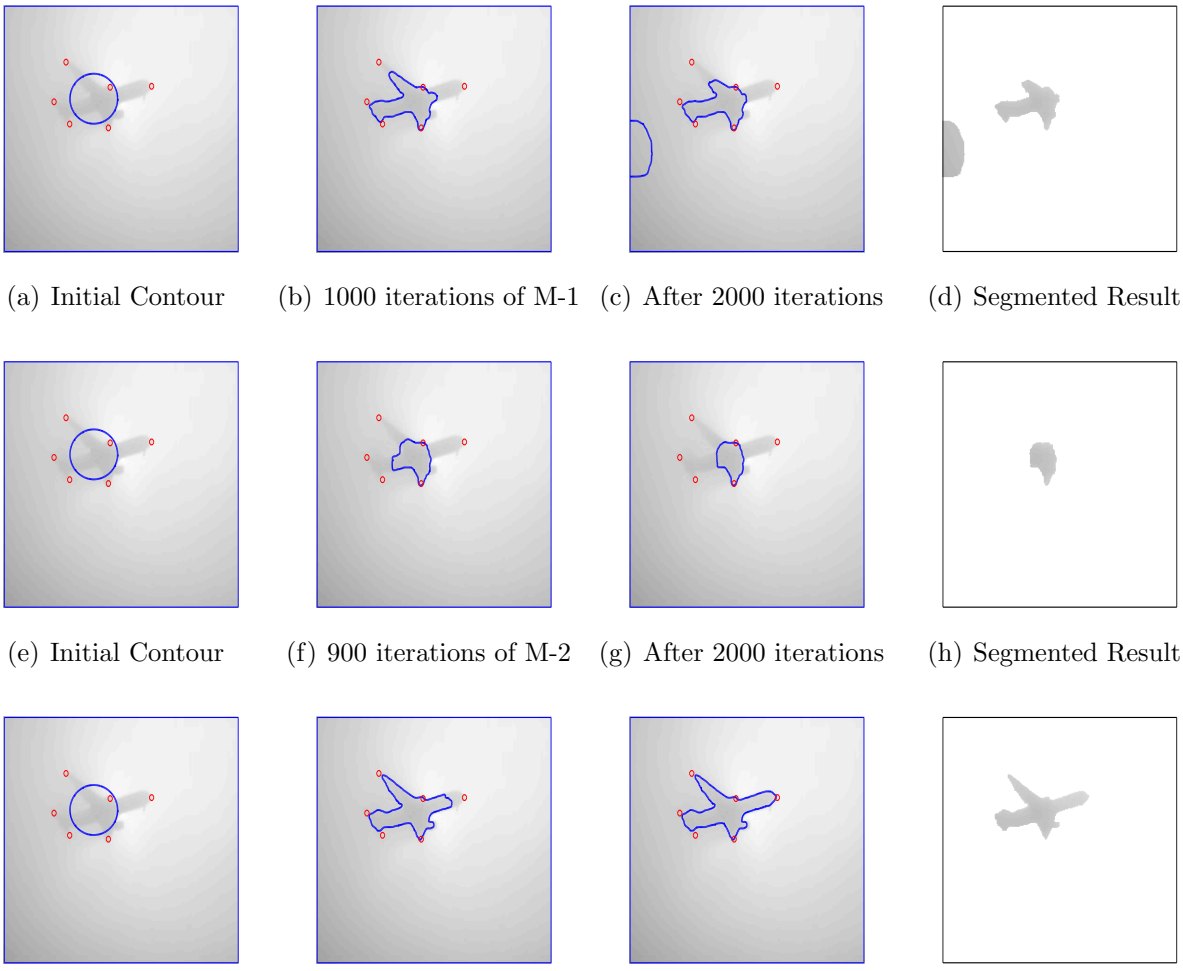

(a) Initial Contour (b) 1000 iterations of M-1 (c) After 2000 iterations (d) Segmented Result

(e) Initial Contour (f) 900 iterations of M-2 (g) After 2000 iterations (h) Segmented Result

(i) Initial Contour (j) 300 iterations of M-3 (k) After 700 iterations (l) Segmented Result

Fig. 7: A figure illustrating the performance of M-1, M-2 and M-3 on a real fog plane image. In contrast with M-1 and M-2, the M-3 successfully completed the task. For M-3, parameters used are: $\lambda = 0.01$, $\mu = 255^2/150000$ and $\sigma = 0.7$.

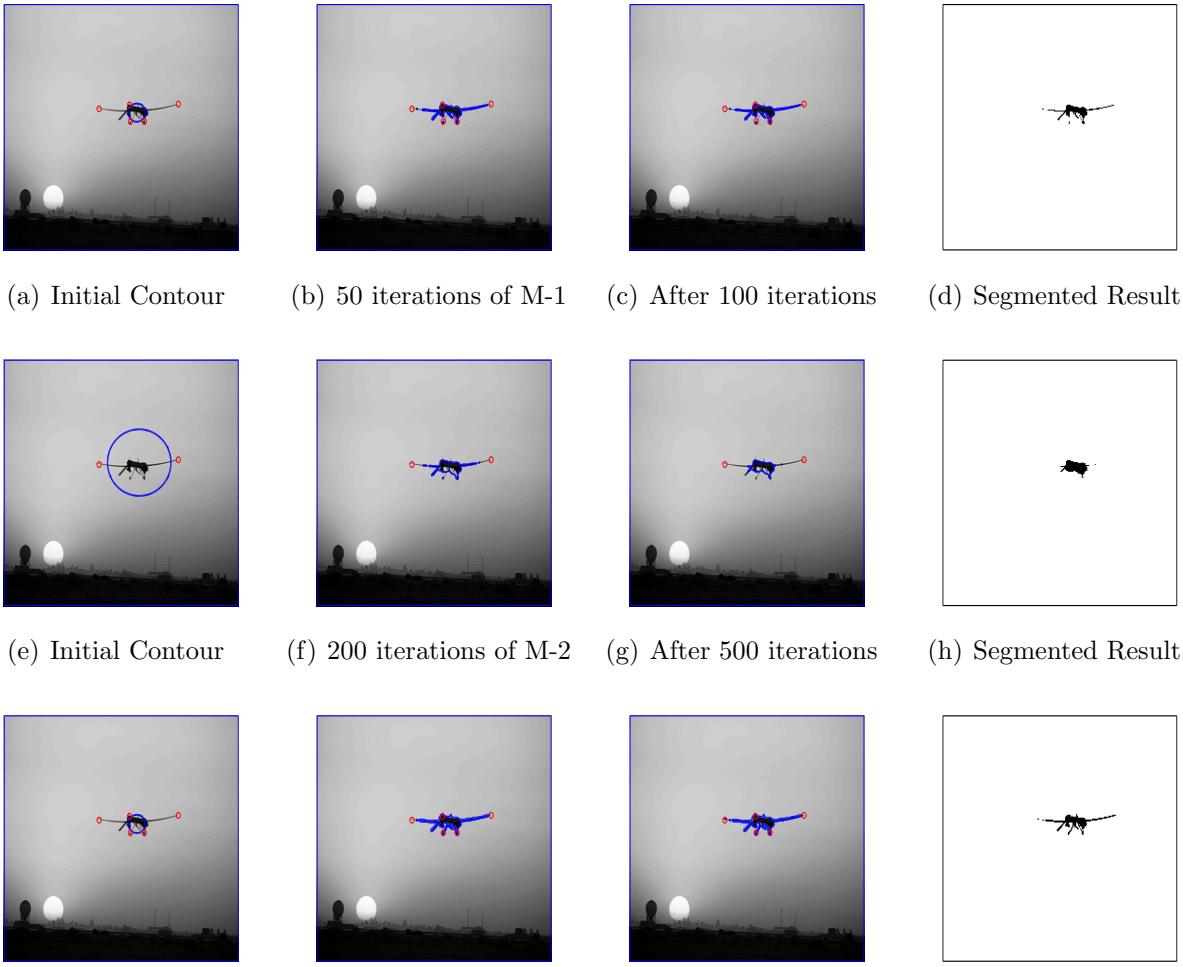

(a) Initial Contour (b) 50 iterations of M-1 (c) After 100 iterations (d) Segmented Result

(e) Initial Contour (f) 200 iterations of M-2 (g) After 500 iterations (h) Segmented Result

(i) Initial Contour (j) 50 iterations of M-3 (k) After 100 iterations (l) Segmented Result

Fig. 8: A figure illustrating the performance of M-1, M-2 and M-3 on a real plane image in sky. In contrast with M-1 and M-2, the proposed M-3 successfully completed the task. For M-3 model parameters used are: $\lambda = 0.1$, $\mu = 255^2/15000$ and $\sigma = 0.01$.

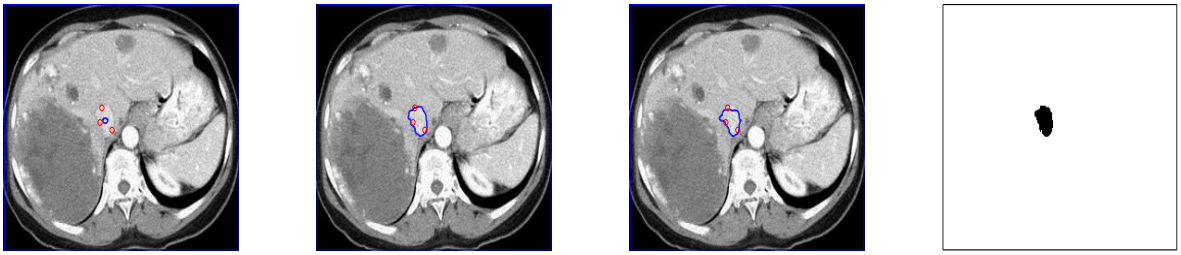

(a) Initial Contour (b) 50 iterations of M-1 (c) After 150 iterations (d) Segmented Result

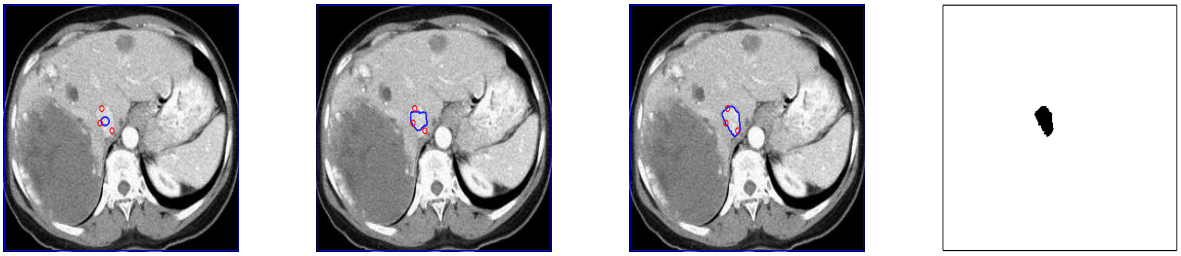

(e) Initial Contour (f) 200 iterations of M-2 (g) After 520 iterations (h) Segmented Result

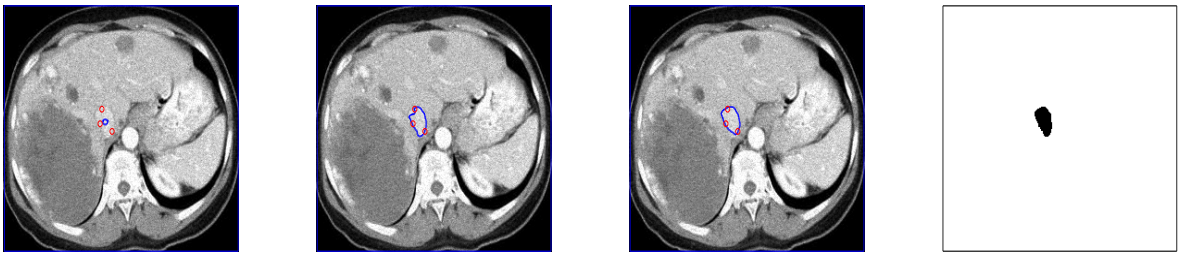

(i) Initial Contour (j) 100 iterations of M-3 (k) After 200 iterations (l) Segmented Result

Fig. 9: A figure revealing the performance of M-1, M-2 and M-3 on real medical abdominal image. It can be easily observed that M-3 successfully captured the region of interest with parameters: $\lambda = 0.0002$, $\mu = 255^2/8000$ and $\sigma = 1$.

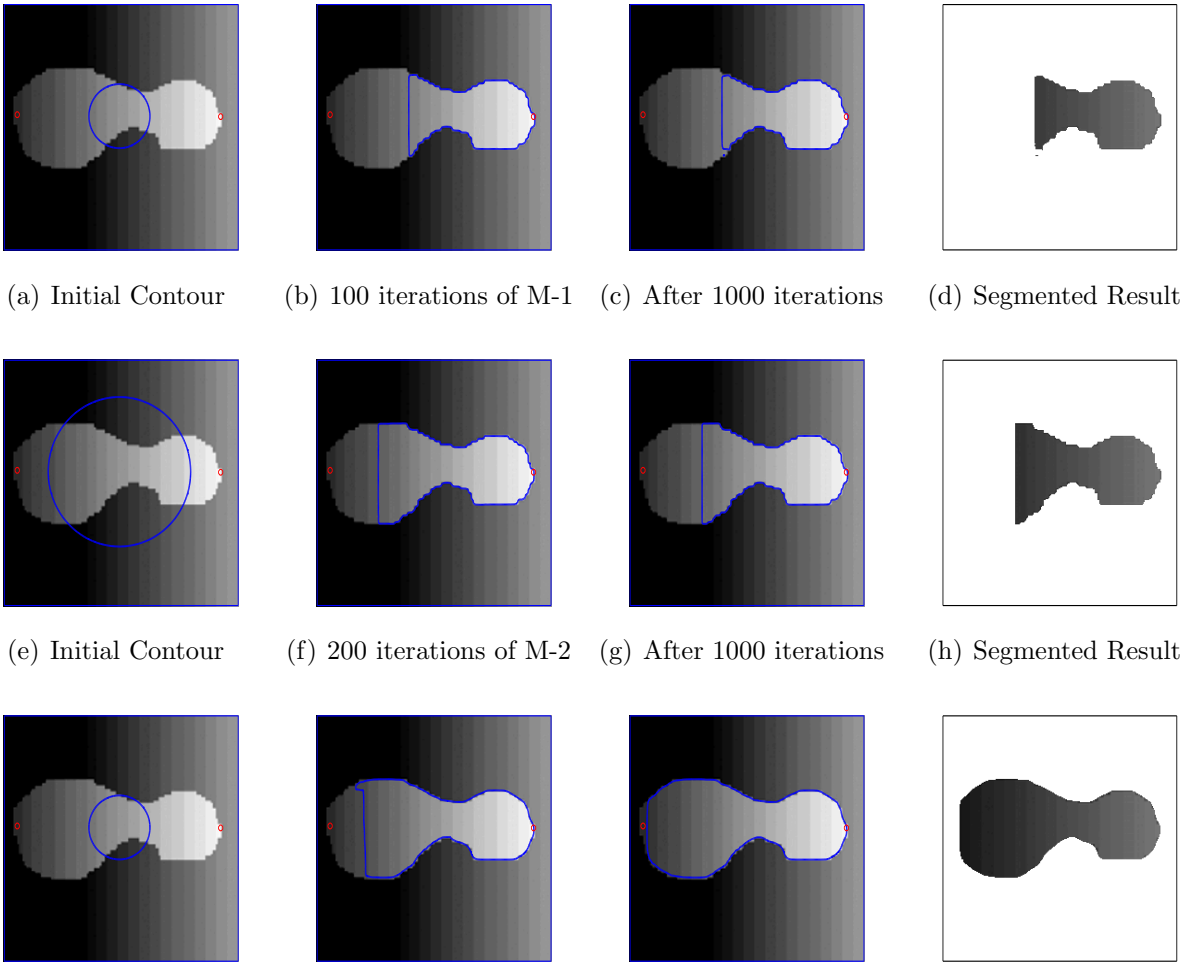

(a) Initial Contour (b) 100 iterations of M-1 (c) After 1000 iterations (d) Segmented Result

(e) Initial Contour (f) 200 iterations of M-2 (g) After 1000 iterations (h) Segmented Result

(i) Initial Contour (j) 100 iterations of M-3 (k) After 250 iterations (l) Segmented Result

Fig. 10: A figure illustrating the performance of M-1, M-2 and M-3 on a synthetic varying intensity image. In contrast with M-1 and M-2, the M-3 successfully completed the task. For M-3 parameters used are: $\lambda = 0.9$, $\mu = 255^2/5000$ and $\sigma = 3$

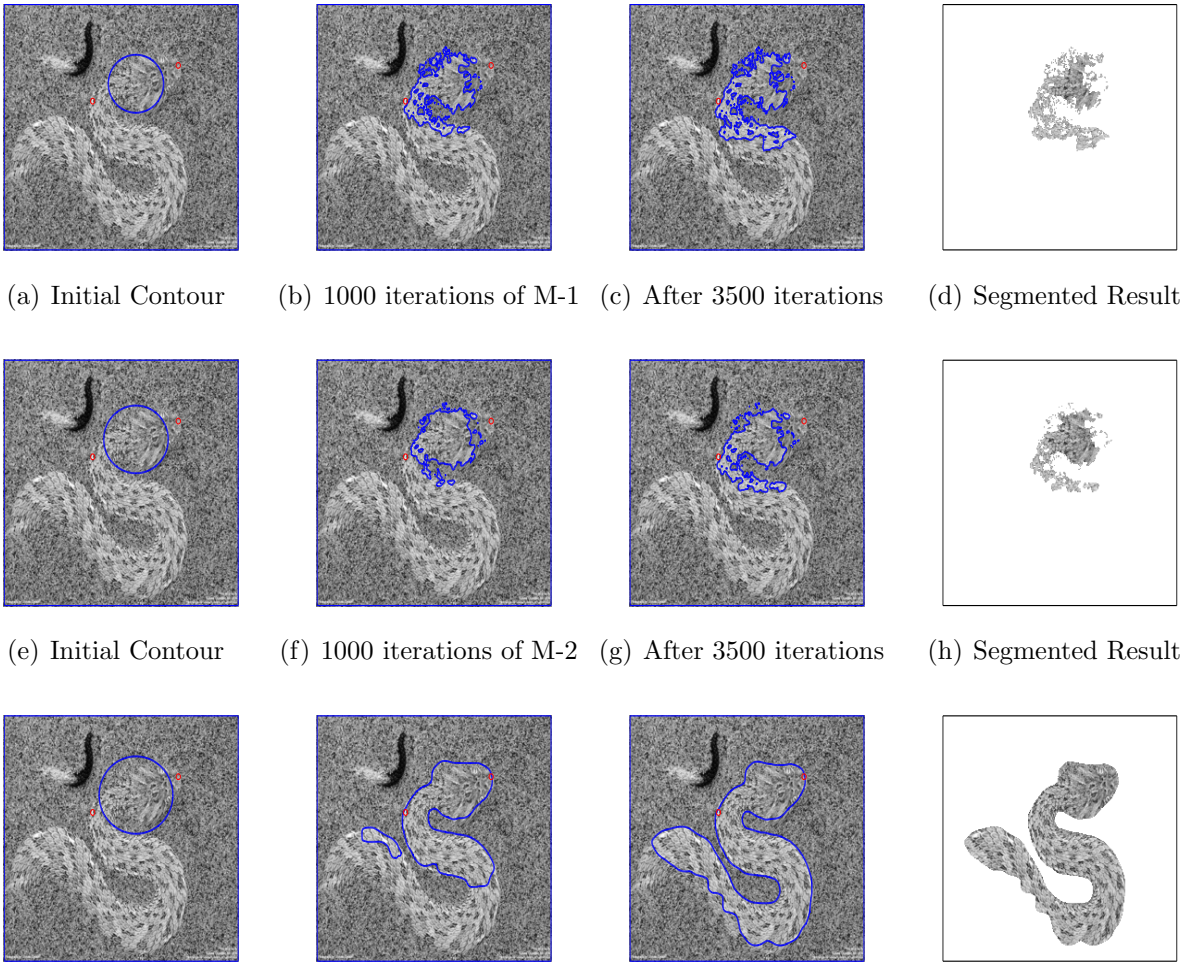

(a) Initial Contour (b) 1000 iterations of M-1 (c) After 3500 iterations (d) Segmented Result

(e) Initial Contour (f) 1000 iterations of M-2 (g) After 3500 iterations (h) Segmented Result

(i) Initial Contour (j) 500 iterations of M-3 (k) After 2700 iterations (l) Segmented Result

Fig. 11: A figure illustrating the performance of M-1, M-2 and M-3 on a real textural snake in sand image. In contrast with M-1 and M-2, the proposed M-3 successfully completed the task. For M-3 model parameters used are: $\lambda = 0.01$, $\mu = 255^2/6000$ and $\sigma = 4.2$.

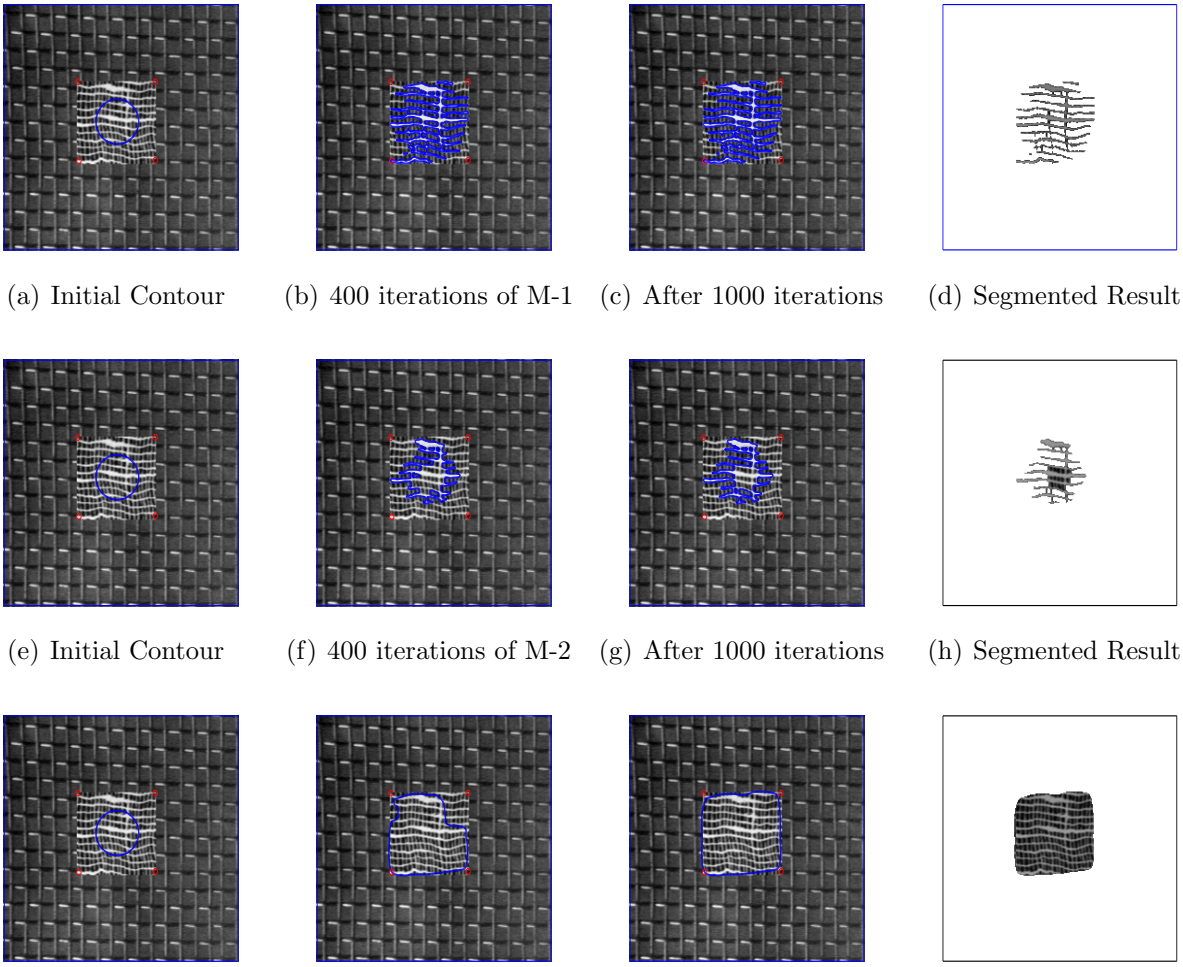

(a) Initial Contour (b) 400 iterations of M-1 (c) After 1000 iterations (d) Segmented Result

(e) Initial Contour (f) 400 iterations of M-2 (g) After 1000 iterations (h) Segmented Result

(i) Initial Contour (j) 100 iterations of M-3 (k) After 300 iterations (l) Segmented Result

Fig. 12: A figure illustrating the performance of M-1, M-2 and M-3 on a textural synthetic image. In contrast with M-1 and M-2, the proposed M-3 successfully completed the task. For M-3 parameters used are: $\lambda = 0.001$, $\mu = 255^2/1000$ and $\sigma = 4$.

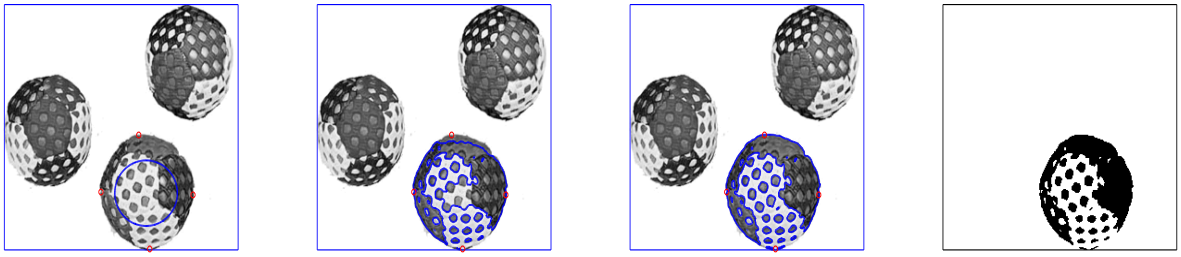

(a) Initial Contour (b) 100 iterations of M-1 (c) After 500 iterations (d) Segmented Result

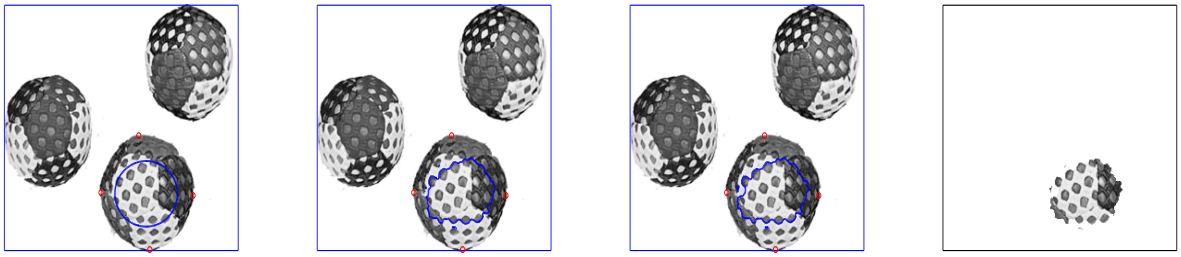

(e) Initial Contour (f) 100 iterations of M-2 (g) After 200 iterations (h) Segmented Result

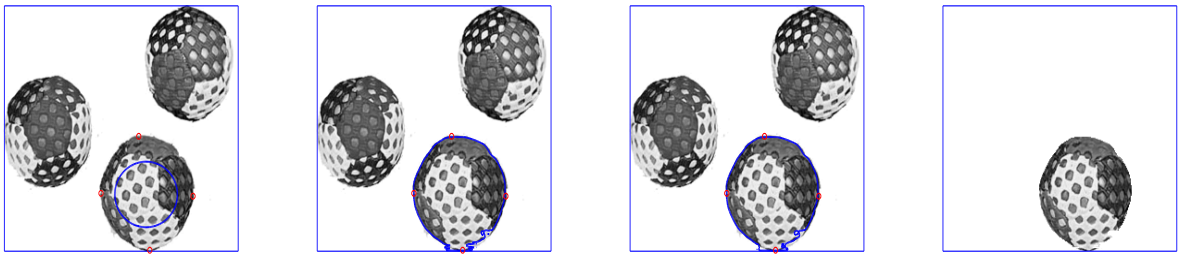

(i) Initial Contour (j) 50 iterations of M-3 (k) After 100 iterations (l) Segmented Result

Fig. 13: A figure illustrating the performance of M-1, M-2 and M-3 on a real textural balls image. In contrast with M-1 and M-2, the proposed M-3 successfully captured the object of interest. For M-3 parameters used are: $\lambda = 0.009$, $\mu = 255^2/30$ and $\sigma = 2.5$.

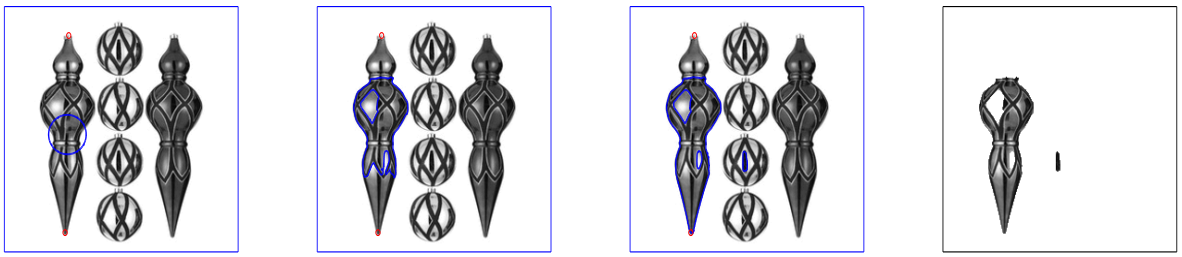

(a) Initial Contour (b) 300 iterations of M-1 (c) After 1000 iterations (d) Segmented Result

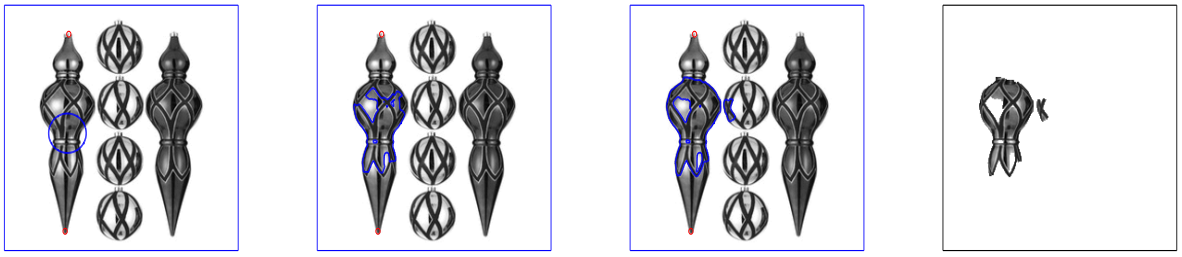

(e) Initial Contour (f) 300 iterations of M-2 (g) After 1000 iterations (h) Segmented Result

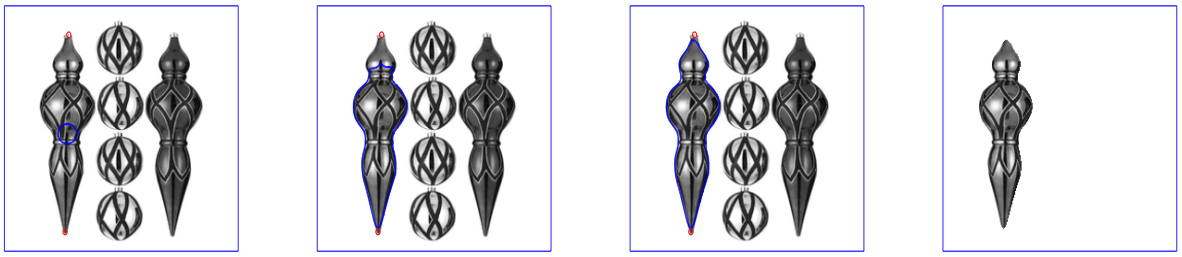

(i) Initial Contour (j) 200 iterations of M-3 (k) After 350 iterations (l) Segmented Result

Fig. 14: A figure showing the performance of M-1, M-2 and M-3 on a real textural image. In contrast with M-1 and M-2, the proposed M-3 completely captured the object of interest. For M-3 parameters used are: $\lambda = 0.009$, $\mu = 255^2/50$ and $\sigma = 2$.

5.1 Performance on Vector-valued Images

To ensure that the proposed model maintains the performance vector-valued images, the M-3 is tested on some real and synthetic hard textural vector-valued images. Firstly, the proposed model is tested on a color images as displayed in figure 15. It can be seen easily that M-3 successfully completed the task by capturing the object of interest in both the images in figure 15. Next, the M-3 is tested on two color medical images of a knee as displayed in figure 16. It can easily observed from the figure 16 that the proposed M-3 successfully captured the slices of interest in the knee images. Secondly, we test the performance of M-3 on real and synthetic color textural images.
Firstly, the M-3 is tested on two synthetic color images as displayed in figure 17. In both the test images in figure 17, the objects of interest involve textural details which can effect the detection of the objects. But, it can be easily observed from the same figure that the proposed M-3 successfully captured the objects of interest. Next, M-3 is tested on a cctv images as displayed in figure 18. It can be easily observed that the proposed M-3 successfully captured the person of interest. Similar result can be witnessed very easily in figures 19 and 20 where the proposed M-3 successfully captured the objects of interest without being effected with the objects interior textural details.

(a) Initial Contour (b) Segmented Result (c) Initial Contour (d) Segmented Result

Fig. 15: A figure exhibiting color images of glasses and birds in which a particular glass and bird are selected and successfully detected using M-3. For M-3 parameters used are: $\lambda = 80$, $\mu = 255^2/150$, $\sigma = 2$ and iteration=100 for 15(a) and $\lambda = 300$, $\mu = 255^2/100000$, $\sigma = 0.1$ and iteration=200 for 15(c).

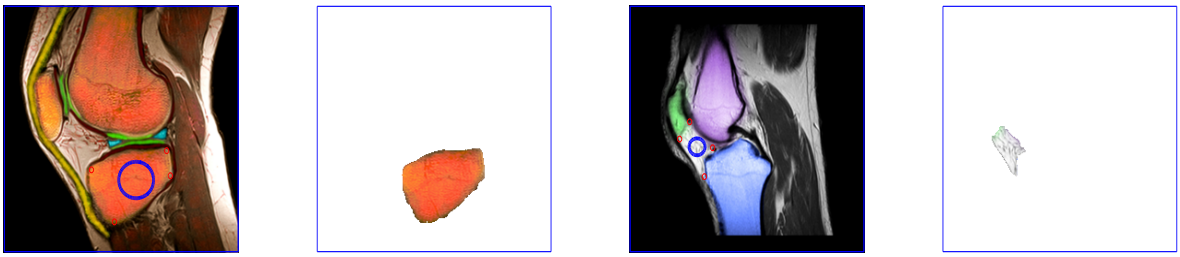

(a) Initial Contour (b) Segmented Result (c) Initial Contour (d) Segmented Result

Fig. 16: A figure displaying color medical images of knee in which particular slices are selected and extracted using M-3. The parameters used are: $\lambda = 90$, $\mu = 255^2/100$, $\sigma = 1$, iteration=180 for 16(a) and $\lambda = 80$, $\mu = 255^2/500$, $\sigma = 0.9$, iteration=500 for 16(c).

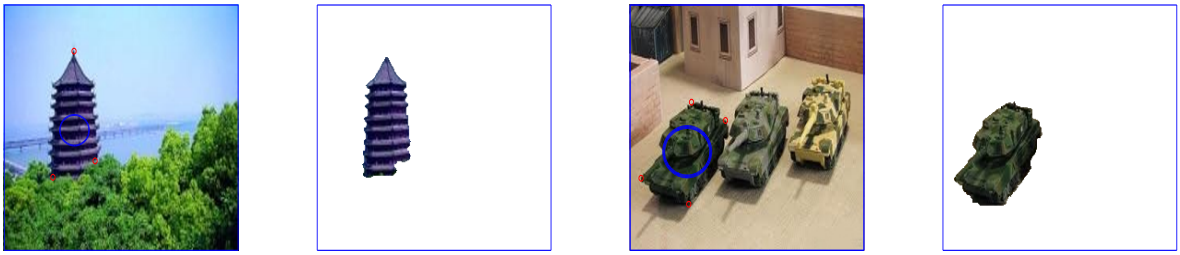

(a) Initial Contour (b) Segmented Result (c) Initial Contour (d) Segmented Result

Fig. 17: A figure displaying real world image having texture and a synthetic tanks image. The M-3 successfully captured the selected objects which are building and tank as clear from 17(b) and 17(d) respectively. The parameters used are: $\lambda = 200$, $\mu = 255^2/500$, $\sigma = 2.5$, iteration=350 for 17(a) and $\lambda = 100$, $\mu = 255^2/500$, $\sigma = 0.9$, iteration=300 for 17(c).

(a) Initial Contour (b) Segmented Result (c) Initial Contour (d) Segmented Result

Fig. 18: A figure exhibiting real cctv images and performance of M-3. It can easily observed that the proposed M-3 extracted the persons of interest. The parameters used are: $\lambda = 150$, $\mu = 255^2/5000$, $\sigma = .5$, iteration=200 for 18(a) and $\lambda = 50$, $\mu = 255^2/800$, $\sigma = 1$, iteration=500 for 18(c).

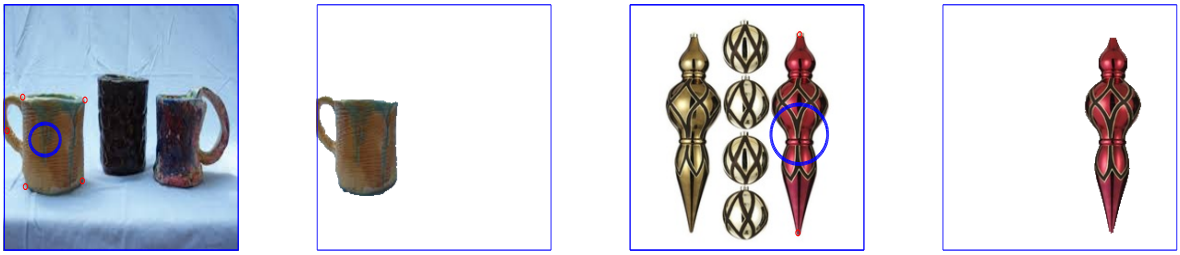

(a) Initial Contour (b) Segmented Result (c) Initial Contour (d) Segmented Result

Fig. 19: A figure displaying a color image of cups, an image of textural objects and the performance of M-3. It can be easily seen from the figure that M-3 successfully captured the cup and object of interest. The parameters used are: $\lambda = 120$, $\mu = 255^2/100$, $\sigma = 0.9$, iteration=700 for 19(a) and $\lambda = 130$, $\mu = 255^2/10$, $\sigma = 2$, iteration=400 for 19(c).

(a) Initial Contour (b) Segmented Result (c) Initial Contour (d) Segmented Result

Fig. 20: A figure exhibiting color synthetic textures images and performance of M-3. M-3 successfully captured the region of interest. The parameters used are $\lambda = 100$, $\mu = 255^2/100$, $\sigma = 3$, iteration=500 for 20(a) and $\lambda = 80$, $\mu = 255^2/50$, $\sigma = 3$, iteration=200 for 20(c).

5.2 Conclusion

A new active contour model for selective segmentation is proposed which can efficiently capture noisy and textural objects of interest. Moreover, the proposed model maintains the efficiency in real world and synthetic color textural images. In future, we plan to extend the proposed algorithm to video segmentation.

References

[1] R. Adams and L. Bischof. Seeded region growing. IEEE Trans. Pattern Analysis and-Machine Intelligence, 16(6): 641-647, 1994.

[2] H. Ali, N. Badshah, K. Chen, G. A. Khan. A Variational Model with Hybrid Images Data Fitting Energies for Segmentation of Images with Intensity Inhomogeneity. Pattern Recognition, http://dx.doi.org/10.1016/j.patcog.2015.08.022.

[3] N. Badshah and K. Chen. Image Selective Segmentation under Geometrical Constraints Using an Active Contour Approach. Math. Comp., 7: 759-778, 2010.

[4] N. Badshah, K. Chen, H. Ali, G. Murtaza. Coefficient of Variation Based Image Selective Segmentation Model Using Active Contours East Asian Journal on Applied Mathematics, 2(2): 150-169, 2012.

[5] J. Bigun, G. H. Grandlund. Optimal orientation detection of linear symmetry, in: Proceedings of the IEEE First International Conference on Computer Vision (ICCV), 433-438, 1987.

[6] J. Bigun, G. H. Grandlund, J. Wiklund. Multi dimensional orientation estimation with applications to texture analysis and optical flow,IEEE Trans. Pattern Anal. Mach. Intell, 13(8): 775-790, 1991.

[7] T. Brox, J. Weickert, B. Burgeth, P. Mrzek. Non linear structure tensors, Image Vis. Comput., 24(1): 41-55, 2006.

[8] V. Caselles, R. Kimmel and G. Sapiro. Geodesic Active Contours. International Jornal of Computer Vision, 22(1): 61–79, 1997.

[9] T. F. Chan and L. A. Vese. Active contours without edges. IEEE Transactions on Image Processing, 10(2): 266–277, 2001.

[10] K. Chen. Matrix Preconditioning Techniques and Applications. Cambridge University Press, first edition, 2005.

[11] C. Gout, C. L. Guyader and L. A. Vese. Segmentation under geometrical conditions with geodesic active contour and interpolation using level set method. Numerical Algorithms, 39: 155–173, 2005.

[12] C. L. Guyader and C. Gout. Geodesic active contour under geometrical conditions theory and 3D applications. Numerical Algorithms, 48: 105–133, 2008.

[13] M. Jeon, M. Alexander, W. Pedrycz, and N. Pizzi. Unsupervised hierarchical image segmentation with level set and additive operator splitting, 26(10): 1461–1469, 2005.

[14] M. Kass, A. Witkin and D. Terzopoulos. Active Contours Models. International Jornal of Computer Vision, 321–331, 1988.

[15] C. Li, R. Huang, Z. Ding, J. C. Gatenby, D. N. Metaxas, J. C. Gore. A level set method for image segmentation in the presence of intensity inhomogeneities with application to MRI, Ieee Transactions on Image Processing, 20(7): 2007–2016, 2011.

[16] C. Li, C. Y. Kao, C. John, Gore and Z. Ding. Implicit Active Contours Driven by Local Binary Fitting Energy. IEEE Conference on Computer Vision and Pattern Recognition (CVPR), pp. 1-7.

[17] T. Lu, P. Neittaanmaki, and X. C. Tai. A parallel splitting up method and its application to Navier-Stokes equations. Appl. Math. Lett., 4(2): 25–29, 1991.

[18] D. Mumford and J. Shah. Optimal approximation by piecewise smooth functions and associated variational problems. Communications on Pure Applied Mathematics, 42: 577–685, 1989.

[19] G. Murtaza, H. Ali and N. Badshah. A Robust Local Model for Segmentation Based on Coefficient of Variation. J. Information & Communication Tech., 5(1): 30-39, 2011.

[20] S. Osher and R. Fedkiw Γ-Level Set Methods and Dynamic Implicit Surfaces, springer verlag, 2003 Lec. Notes Comp. Sci., 3708: 499–506, 2005.

[21] S. Osher and J. A. Sethian. Fronts propagating with curvature-dependent speed: algorithms based on Hamilton-Jacobi formulations. J. Comput. Phys., 79(1): 12–49, 1988.

[22] L. A. Vese and T. F. Chan. A multiphase level set framework for image segmentation using the Mumford and Shah model, Int. J. Computer Vision, 50(3): 271–293, 2002.

[23] L. A. Vese. Multiphase object detection and image segmentation. Technical report, UCLA Dept. of Math., CAM 02–36, 2002.

[24] L. Vincent and Soille. Watersheds in Digital Spaces - an efficient algorithm based on immersion. IEEE Trans. Pattern Analysis and Machine Learning, 6: 583–598, 1994.

[25] B. Wang, X. Gao, D. Tao and X. Li, A Unified Tensor Level Set for Image Segmentation. Ieee Transection on Systems, Man, and Cybernaticspart B: Cybernatics, 40(3): 857–867, 2010.

[26] B. Wang, X. Gao, D. Tao and X. Li, A Nonlinear Adaptive Level Set for Image Segmentation. Ieee Transaction on Cybernatics, 44(3): 418–428, 2014.

[27] B. Wang, X. Gao, D. Tao and X. Li, A Unified Tensor Level Set for Image Segmentation. Ieee Transection on Systems, Man, and Cybernaticspart B: Cybernatics, 40(3): 857–867, 2010.

[28] X. F. Wang, D. S. Huanga, H. Xu. An efficient local ChanVese model for image segmentation. Pattern Recognition, 43: 603–618, 2009.